

Effects of cylinder array height on tracked vortex packets in a turbulent boundary layer

Yan Ming Tan

Department of Aerospace Engineering and Mechanics
University of Minnesota, Minneapolis MN, 55455 USA
tanxx247@umn.edu

Ellen K. Longmire

Department of Aerospace Engineering and Mechanics
University of Minnesota, Minneapolis MN, 55455 USA
longmire@umn.edu

ABSTRACT

The effect of obstacle height was investigated for cylindrical arrays embedded within the log region of a turbulent boundary layer with $Re_\tau = 2500$. The array spacing was set at 0.6δ to match the most probable spanwise spacing of hairpin packets. An array that extended to the top of the log region ($H^+ = 500$) strongly amplified the 0.6δ mode throughout the log region with the strongest relative amplification closest to the wall at $z^+ = 125$. A shorter array with $H^+ = 125$ affected the flow up to $z^+ = 300$ such that energy contained in spanwise scales below 0.6δ was decreased and energy in larger spanwise scales was increased. Cross correlation of flying PIV fields suggested that the shorter array enhanced the streamwise alignment of incoming packet structures in contrast to the taller array which shifted incoming packets into spanwise zones midway between the cylinders.

INTRODUCTION

Many studies (e.g. Adrian *et al.*, 2000) have shown that coherent eddies within wall bounded flows organize into groups termed as hairpin packets. A packet includes multiple hairpin-like vortices aligned in the streamwise flow direction and moving at approximately the same velocity. These packets are thought to be a key contributor to drag within wall bounded flows (Ganapathisubramani *et al.*, 2003); hence perturbing these structures could be a viable method of manipulating boundary layer characteristics.

Previous work aimed at perturbing boundary layer behavior can be loosely categorized as (a) disrupting the near wall cycle of turbulent production and (b) breaking up the larger scale coherent eddies within the boundary layer. Generally, rough walls are thought to disrupt the near wall cycle of turbulence production. Streamwise riblets have been shown to reduce skin friction by up to 7-10% (Bechert *et al.*, 1997). Recent experiments by Nugroho *et al.* (2013), using converging/diverging riblet orientations, yielded a substantial effect on the overall boundary layer structure

despite the riblets being only 1% of the unperturbed boundary layer thickness. In this study and most other studies on roughness, the streamwise extent of the perturbation is much longer than in the present study. Recent studies examining perturbations of height much less than δ with limited streamwise extent include Jacobi & McKeon (2011) (one spanwise bar) and Guala *et al.* (2012) (periodic array of hemispheres).

Many studies on large-eddy break up (LEBU) devices were conducted in the 1970's. Corke *et al.* (1981), utilizing ribbon-like devices with large wall normal extent ($H/\delta = 0.2$), reported skin friction drag reduction of 30–40%. The goal of LEBUs was similar to the current study, which is to affect the larger scale coherent structures within the flow. A difference between the present study and most previous ones is that LEBU devices are typically on the order of δ .

In the current work, a spanwise array of cylinders was used to perturb the packets within the boundary layer. The wake behind finite wall-mounted cylinders is highly three dimensional and can include free end tip vortices, Karman-like vortices along most of the cylinder height, and a horseshoe vortex near the base (Pattenden *et al.*, 2005). Relevant parameters that strongly affect the wake are cylinder height with respect to boundary layer thickness, H/δ (Park & Lee 2002; Hain *et al.*, 2008), inflow condition; laminar or turbulent (Wang *et al.*, 2006), and cylinder aspect ratio (Sumner *et al.*, 2004).

Previously, Ryan *et al.* (2011) considered cylinder arrays immersed within the log region of a boundary layer ($Re_\tau = 1200$) using hot-wire anemometry. Both 0.26δ and 0.5δ spaced arrays shifted the peak in turbulence intensity away from the wall and towards the top of the log region. Changes in mean velocity remained confined to the log region. In contrast, RMS perturbations persisted beyond the log region at $x/\delta = 7$. (Tan, 2013). Similar behaviour in the mean velocity was observed by Tomkins (2001) downstream of hemispherical obstacles embedded in a boundary layer with $Re_\tau = 2200$.

Ortiz-Duenas *et al.* (2011) investigated array spacings of 0.2δ and 0.4δ with PIV and V3V at $Re_\tau = 2500$ and found significant spanwise interactions between adjacent cylinder wakes with the 0.4δ spacing resulting in a relatively stable wake structure. More recently, Zheng *et al.* (2014) considered spacings up to 0.8δ with a height of $H^+ = 500$ (0.2δ) at $Re_\tau = 2500$ and showed that a 0.6δ array can reinforce existing packet structures resulting in a persistent downstream signature. This array spacing matched the dominant natural scaling of packet structures found by Hutchins *et al.* (2005) and Tomkins and Adrian (2003).

In the present work, we document the wall normal variation of effects downstream of the 0.6δ array considered by Zheng *et al.* (2014) and compare these results against those for an array of reduced height.

METHODOLOGY

Experiments were conducted in a water channel facility at $Re_\tau = 2500$. The test section length and span were 8 m and 1.22 m, and the water depth was 0.39 m. Flow conditioning was applied through a series of screens and a honeycomb section followed by a 5:1 asymmetric contraction. A 3 mm trip wire was mounted on the bottom wall at the beginning of the test section, and the flow developed for 5 m prior to the measurement domain. The freestream velocity U_∞ was 0.51 m/s, and the unperturbed boundary layer thickness δ was 125 mm at the array location. The freestream turbulence level was measured as 1.4%. More details on the facility can be found in Gao *et al.* (2011).

Two array heights were considered as shown in Table 1. Cylinder diameter was $D^+ = 125$. The spacing between the array elements was 0.6δ posing a frontal blockage within the boundary layer as documented in Table 1.

Table 1. Array heights for the two types of cylinders.

Type	H/δ	H^+	Blockage
Short	0.05	125	0.42%
Medium	0.2	500	1.70%

Particle Image Velocimetry (PIV) measurements were conducted in wall-parallel planes at three heights: $z^+ = 125$, 300, 500. Measurement planes were illuminated by a Spectra Physics dual head Nd:YAG laser with pulse energy of 370 mJ. The laser sheet thickness was approximately 1 mm. Images were captured by 12 bit TSI PowerView 4MP Plus cameras with 2048 x 2048 pixels. The flow was seeded with silver coated hollow glass spheres with an average diameter of 13 μm .

Fixed PIV measurements were conducted over a streamwise range of $0 < x/\delta < 7$ where zero corresponds to the array location. Stereoscopic PIV (SPIV) and Planar PIV (PPIV) measurements were performed. The field of view (FOV) for SPIV was $1.1\delta \times 1.1\delta$. A wider field, $1.1\delta \times 1.9\delta$, was obtained for PPIV to resolve larger scale spanwise variations of velocity. Flying PIV was conducted over a streamwise range of $-2 < x/\delta < 7$ to track the downstream

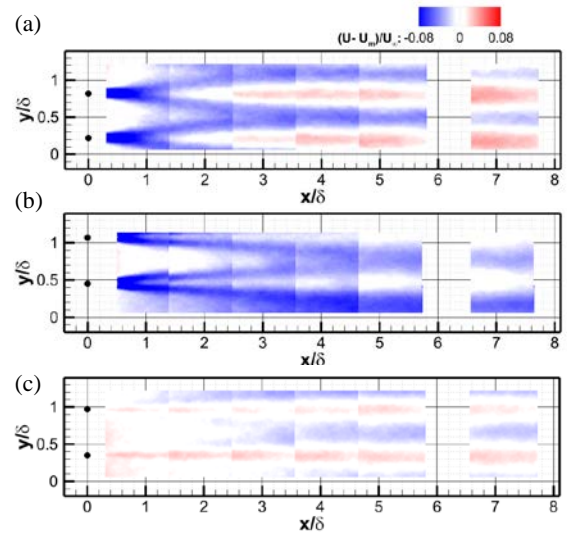


Figure 1. Medium array. Average deviation of streamwise velocity from unperturbed local mean at (a) $z^+ = 125$, (b) $z^+ = 300$, and (c) $z^+ = 500$, normalized by $U_\infty = 0.51$ m/s. Spatial variables normalized by $\delta = 125$ mm measured at $x = 0$. Flow is from left to right.

evolution of flow structures approaching the array. The measurement system was traversed at the local mean velocity at the measurement height. A total of 45 runs were conducted for each case.

Dominant spanwise modes based on the streamwise velocity component were extracted from PIV vector fields by a Fourier based method described in Zheng *et al.* (2014). Autocorrelations were performed on the fixed PIV measurements from sets of 1000 independent samples. Cross correlations were obtained from $1.1\delta \times 1.9\delta$ size fields acquired by flying PIV.

The statistical uncertainty of instantaneous PIV vectors was computed to be 0.8%, 0.9% and 1.6% of U_∞ for U , V and W components respectively in SPIV and 1.1% of U_∞ for both velocity components in PPIV. The largest uncertainty in averaged SPIV and PPIV results was 0.5%.

RESULTS

Medium Array

The average deviation of the local streamwise velocity from the unperturbed mean velocity downstream of the medium array ($H^+ = 500$) is plotted in Figure 1 for the three measurement heights: $z^+ = 125$, $z^+ = 300$ and $z^+ = 500$. The wake pattern at $z^+ = 125$ was similar to the results of Zheng *et al.* (2014) at $z^+ = 300$ shown in Figure 1b. At both z^+ locations, a deficit occurs directly behind each cylinder. Notably, the deficits fill in sooner at $z^+ = 300$ than at $z^+ = 125$ ($x/\delta \sim 0.9$ vs. 1.2), such that the fluid then moves fastest in the locations directly behind the cylinders. This faster moving fluid results from the net downwash generated by tip vortices shed off of the free end of each cylinder. On average, each cylinder wake splits. Then each half merges

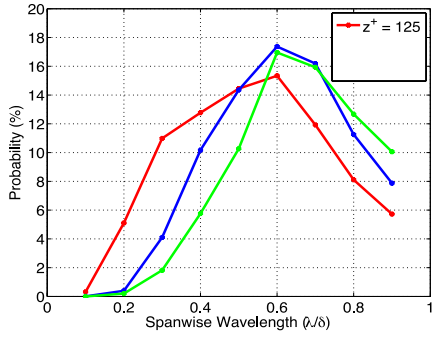


Figure 2. Unperturbed flow at $x/\delta = 0$. Dominant spanwise modes.

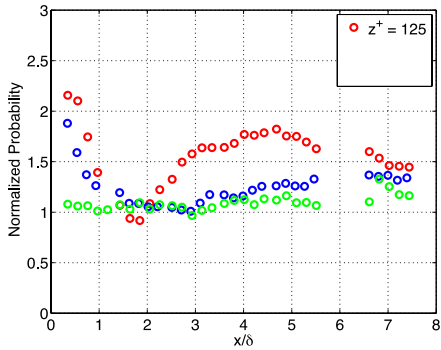


Figure 3. Medium array. Normalized probability of 0.6δ as the dominant spanwise mode. Normalized probability of 1 is equivalent to the probability in unperturbed flow.

with its neighbor to form a low momentum region (LMR) in each mid span location. The LMR's then persist beyond the end of the measurement region at both measurement heights. The merging occurred earlier at $z^+ = 125$ ($x/\delta \sim 2.5$) than at $z^+ = 300$ ($x/\delta \sim 3.5$). The LMR was weaker at $z^+ = 125$ ($0.02U_\infty$) than at $z^+ = 300$ ($0.05U_\infty$) at $x/\delta = 7$. On the other hand, the faster moving regions were stronger at $z^+ = 125$ ($0.035U_\infty$) compared to $z^+ = 300$ ($0.005U_\infty$).

Figure 1c, which shows the mean velocity deviation at the cylinder tip height, $z^+ = 500$ is notably different. First, the fluid directly behind each cylinder is moving faster than in unperturbed flow by $\sim 0.02U_\infty$. Second, these fast moving regions persisted through the measurement domain. Inspection of instantaneous spanwise velocity fields indicated a converging pattern directly behind the cylinder tips whereas Karman-like patterns were observed at $z^+ = 125$ and 300. Stereo PIV measurements (not shown) indicate significant downwash induced by the tip vortices which was stronger on average at $z^+ = 500$ ($0.11U_\infty$) than at $z^+ = 300$ ($0.08U_\infty$) directly behind each cylinder. The converging spanwise velocity in combination with the local downwash helps explain the faster moving fluid in-line with the cylinder spanwise positions.

The spanwise variation of streamwise velocity was examined in individual PIV fields to determine the dominant wavelengths of variation. The dominant modes were sorted with a bin size of 0.1δ for all samples starting from fields of

view with length vs. span of $1.1\delta \times 1.9\delta$. Modes exceeding 0.9δ suffer from attenuation due to the limited FOV and therefore are not plotted. PDFs of the dominant spanwise modes for the unperturbed flow are shown in Figure 2. At $z^+ = 125$, smaller wavelengths were more prominent compared to the locations further from the wall. With increasing wall-normal distance, the PDFs shift gradually toward larger wavelengths. Nevertheless, the 0.6δ mode was the most probable dominant scale at all three measurement heights. This peak value, which is consistent with similar analysis by Hutchins *et al.* (2005) at $z/\delta = 0.14$ for $Re_\tau = 1100$, can be inferred as the most probable spanwise spacing between hairpin packets.

The streamwise evolution of the 0.6δ mode probability behind the medium array is plotted in Figure 3. The most striking trend is that the 0.6δ mode was amplified at all three measurement heights. At $z^+ = 125$, the mode was initially high directly behind the array and decayed with downstream distance. It falls to a minimum at $x/\delta \sim 2$, then increases to 1.8 times the unperturbed value at $x/\delta \sim 5$, before decreasing again. At the last measurement zone, the amplification was still strong at 1.5 times the local unperturbed 0.6δ mode. Data at $z^+ = 300$ reproduced from Zheng *et al.* (2014) shows similar but weaker variations. The probability was initially high but decreased more gradually with downstream distance until a weaker minimum occurred at the later position of $x/\delta \sim 3$. This trend is consistent with the average streamwise fields showing a later merging location compared to $z^+ = 125$. After incoming packets interact with neighboring cylinder wakes, they tend to migrate toward the midspan location between cylinders consistent with the rise and persistence of the 0.6δ mode (see Zheng *et al.*, 2014). The current results at $z^+ = 125$ suggest stronger wake interactions initially followed by a very significant enhancement of the 0.6δ mode. When the 0.6δ mode reached a minimum, the 0.3δ mode (not shown) increased to a maximum. The 0.3δ mode was most likely enhanced due to the splitting of the wakes in this region. This effect was similar but weaker at $z^+ = 300$. At the array tip height ($z^+ = 500$), the 0.6δ mode appears to increase gradually starting at $x/\delta \sim 3$ reaching a value near 1.3 at $x/\delta \sim 7$. Measurements further downstream are needed to document the full streamwise extent of the array's effects.

Short array

The average wake pattern behind the tips of the shorter array ($z^+ = 125$, $H^+ = 125$) was qualitatively similar to that behind the medium array ($z^+ = 500$, $H^+ = 500$). The average downwash immediately behind the shorter cylinders was weaker ($0.05U_\infty$) than that behind the medium cylinders ($0.08U_\infty$). The average increase in streamwise velocity at these locations was slightly larger for $H^+ = 125$ ($0.03U_\infty$) than for $H^+ = 500$ ($0.02U_\infty$). Figure 4 illustrates the converging spanwise velocity directly behind the cylinder tips at $z^+ = 125$, where the qualitative trends were similar for $H^+ = 500$, $z^+ = 500$. The figure shows that the average effect lasted over a distance of 0.5δ behind the short array where the same effect was measurable over a distance of 3δ behind the medium array. A similar but weaker converging

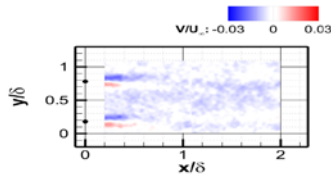


Figure 4. Short array. Average spanwise velocity at $z^+ = 125$.

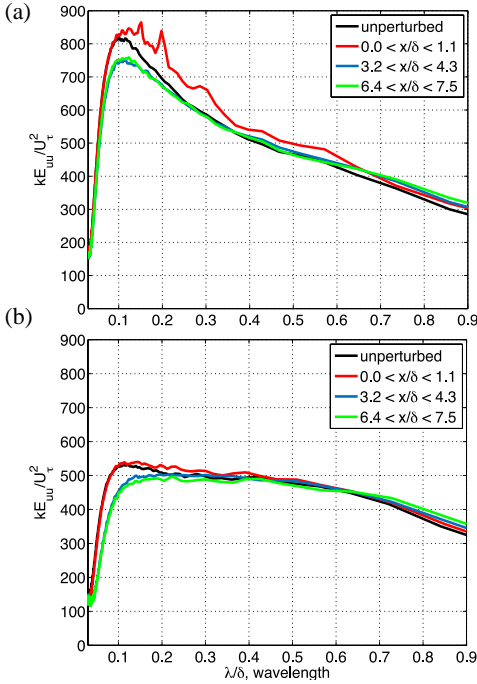


Figure 5. Short array. Premultiplied spectra of spanwise variation in streamwise velocity: (a) $z^+ = 125$ and (b) $z^+ = 300$. The unperturbed spectrum at $x/\delta = 0$ is shown in black.

effect was observed downstream of the short array at $z^+ = 300$ (not shown). Furthermore, plots of average streamwise velocity indicate faster moving regions directly behind the shorter cylinders at both $z^+ = 125$ and 300 , with a weaker effect at $z^+ = 300$ ($0.008U_\infty$) than at $z^+ = 125$ ($0.03U_\infty$). These results thus suggest that the perturbation extended well beyond the array height. Measurements at $z^+ = 500$, corresponding to the top of the log region, yielded no significant changes in mean velocity compared to the unperturbed flow.

The dominant spanwise modes downstream of the short array were extracted, but no clear trend was observed vs. the unperturbed flow. However, premultiplied spectra of the spanwise variation of streamwise velocity did show some measureable trends. Figure 5a shows premultiplied spectra downstream of the short array measured at $z^+ = 125$, the array tip height. Initially, the energy increased at all wavelengths compared to the unperturbed, and multiple peaks are present. Further downstream, the energy decreases in all scales smaller than 0.6δ while it increases at larger wavelengths. Figure 5b shows the premultiplied spectra at z^+

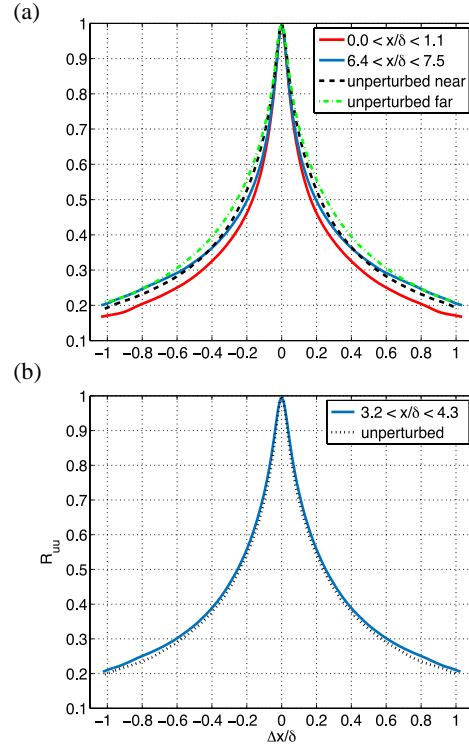


Figure 6. Short array. Autocorrelation of streamwise velocity at (a) $z^+ = 125$ and (b) $z^+ = 300$. Near: $0.0 < x/\delta < 1.1$ and Far: $6.4 < x/\delta < 7.5$. Figure 6b unperturbed at $3.2 < x/\delta < 4.3$

$= 300$, beyond the array height. The trends are similar to Figure 5a, but the initial increase in energy is weak. Further downstream, the energy shifts from smaller to larger scales similar to the result at $z^+ = 125$.

Plots of the streamwise autocorrelation of streamwise velocity downstream of the short array are shown in Figure 6. At $z^+ = 125$, the streamwise coherence is reduced immediately downstream of the array. Further downstream, the correlation recovers toward the unperturbed shape. At $z^+ = 300$, the correlation first matches the unperturbed case, but then is enhanced beginning at the zone centered at $x/\delta = 3.8$ where the streamwise coherence increased (see Figure 6b). This trend is expected as it would take some distance for the array's effect to be felt higher up. At the last measurement zone ($x/\delta = 7$, not shown), the streamwise coherence remained slightly enhanced.

The results for the short array can be contrasted with those behind the medium array (not shown because of space limitations). At $z^+ = 125$, the autocorrelation downstream of the medium array showed enhanced streamwise coherence beginning at $x = 2\delta$ corresponding to the location of average wake merging (Figure 1a). A similar weaker enhancement occurred beginning at $x/\delta = 3$ at $z^+ = 300$ consistent with the later merging of wakes in averaged streamwise velocity (Figure 1b).

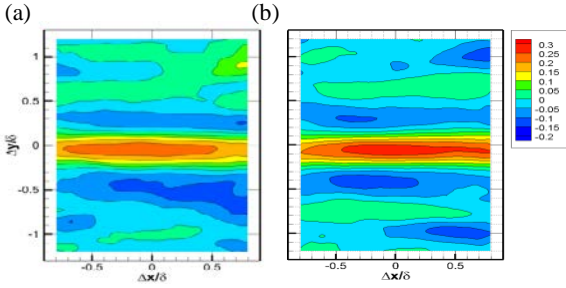


Figure 7. Cross correlation of streamwise velocity between fields centered at $x/\delta = -0.5$ and $x/\delta = 7.2$ for (a) unperturbed (b) short array at $z^+ = 300$.

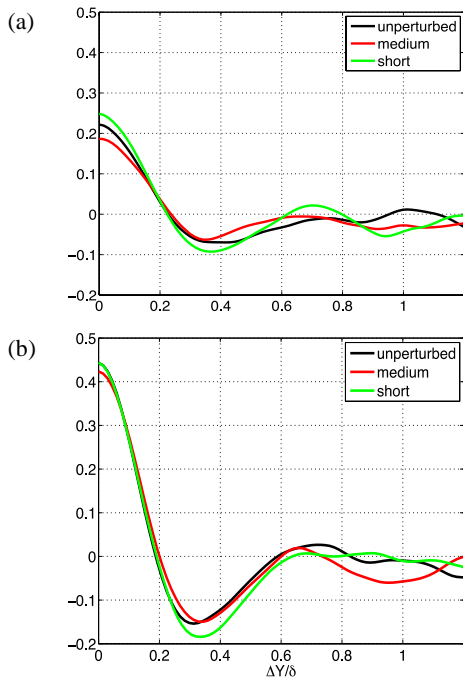


Figure 8. Cross correlation of streamwise velocity at $z^+ = 300$ for (a) field centered at $x/\delta = -0.5$ with field centered at $x/\delta = 7.2$ and (b) field centered at $x/\delta = 4.8$ with $x/\delta = 7.2$.

Flying PIV results (medium and short arrays)

The incoming packet organization was compared with the flow organization downstream of the array both visually and via cross correlation. The stations chosen for the cross correlation were the unperturbed field upstream of the array and the field furthest downstream of the array. Figure 7 shows cross correlation maps of the streamwise velocity at $z^+ = 300$ for the unperturbed flow and the short array. Interestingly above the shorter array, the streamwise coherence was enhanced compared to that in the unperturbed flow. This result was supported by observations of the instantaneous flying runs at $z^+ = 300$ whereby the spanwise meandering of the LMRs downstream of the short array appeared to be suppressed in certain runs. The cross

correlation map for the medium array at $z^+ = 300$ (not shown) indicated a smaller but noticeable enhancement of streamwise coherence versus the unperturbed. This smaller enhancement may result from the LMRs migrating to the mid spacing location downstream of the array (see Zheng *et al.*, 2014). This migration causes a mismatch in the streamwise alignment of most of the structures hence a reduction in the peak of the streamwise correlation. Figure 8a compares the spanwise variation at the center of the cross correlation maps ($\Delta X = 0$) shown in Figure 7 with the same result from the medium array. The positive correlation is wider in span for the medium array which could be due to a smearing effect caused by LMRs at all incoming locations tending to migrate to the mid span location. Such spanwise migration was not obvious for LMRs encountering the short array. On the other hand, the cross correlation for the short array suggests that the spanwise periodicity of the flow was enhanced compared to the unperturbed flow as a local outer maximum was observed at $\sim 0.7\delta$ in Figure 8a. Moreover, the first negative lobe of this correlation was stronger than in the other two correlations, which could also result from enhanced stability and spanwise periodicity.

A second set of cross correlations is shown in Figure 8b, whereby two locations downstream of the array are correlated. The first location is chosen to coincide with the streamwise location downstream of the medium array where LMRs have, on average, already shifted into the mid-span positions between cylinders (see Figure 1). In this case, all of the correlations show stronger peaks at $\Delta Y = 0$ displacement as well as stronger first negative lobes as might be expected due to the reduced distance between correlated fields. The peak corresponding with the medium array now matches with that for unperturbed flow, while the peak corresponding with the short array is slightly higher. The first zero crossing moves to smaller ΔY for all three cases, also as expected, with the medium array still showing the largest zero crossing value. Moreover, the medium array correlation shows the strongest periodicity with a second local maximum occurring near 0.95δ . These results suggest that, once LMRs are redirected by the medium array, they maintain a more stable spacing until the end of the measurement domain compared with flow downstream of the short array or unperturbed flow. Meanwhile, the correlation downstream of the shorter array has the strongest negative lobe near $\Delta Y/\delta = 0.3$ as in Figure 8a, again supporting the idea that the shorter array slightly suppressed spanwise meandering of flow structures as seen in instantaneous runs of the flying PIV measurements.

CONCLUSIONS

The effect of obstacle height was investigated for arrays embedded within the log region of a turbulent boundary layer with $Re_\tau = 2500$. The array spacing was set at 0.6δ to match the most probable natural spanwise spacing of hairpin packets. Measurements downstream of an array extending to the top of the log region ($H^+ = 500$) yielded wake patterns at $z^+ = 125, 300, \text{ and } 500$ driven by an average downdash

downstream of each cylinder. In these locations, flow converged in the spanwise direction at the cylinder tips, and moved toward the wall bringing higher momentum fluid downward. This averaged secondary motion led to wake splitting and eventually faster streamwise velocity directly behind each cylinder, with this occurring sooner at $z^+ = 300$ than at 125. These results are consistent with the flow structure downstream of individual finite cylinders observed by Pattenden *et al.* (2005). The dominant spanwise scale of 0.6δ corresponding to the natural spanwise packet scaling was amplified at all three measurement heights by this medium array with the relative amplification strongest at the location closest to the wall.

Measurements downstream of an array with reduced height ($H^+ = 125$) yielded a wake pattern at the tip height similar to that at the medium array tip height ($H^+ = 500$), with a converging region of fluid behind the cylinders and a slight increase in streamwise velocity. This effect was weaker for the shorter array compared to the medium even when normalized by the local unperturbed mean velocity. Spectra of spanwise variations in streamwise velocity showed that, downstream of this array, energy shifted from smaller to larger wavelengths at both $z^+ = 125$ and 300. Scales below 0.6δ were eventually suppressed and scales greater than or equal to 0.6δ were amplified compared with unperturbed flow. Autocorrelations of streamwise velocity showed that streamwise coherence was increased at $z^+ = 300$ starting at a distance of 3δ behind the array. Thus perturbations from the shorter array extended well beyond its wall normal height, consistent with results by Tomkins (2001).

Cross correlations and instantaneous visualizations from flying PIV suggested that the short array enhanced alignment of or suppressed meandering of existing streamwise structures in the log region compared to unperturbed flow. This result contrasted with flow downstream of the medium array which tended to direct LMRs into the region midway between cylinders.

Future work will include measurements farther downstream to investigate the extent of the medium array's effects. Furthermore, conditional cross correlations can be performed on the flying PIV data set to further understand the array's effects on incoming packet structures.

REFERENCES

Adrian, R.J., Meinhart, C.D., and Tomkins, C.D. 2000. "Vortex organization in the outer region of the turbulent boundary layer." *J. Fluid Mech.* **422**:1–54.

Bechert, D.W., M. Bruse, W. Hage, J. G. T. Van Der Hoeven, and G. Hoppe. 1997. "Experiments on drag-reducing surfaces and their optimization with an adjustable geometry." *J. Fluid Mech.* **338**:59–87.

Corke, T.C., Guezennec Y., and Nagib, H.M. 1981. "Modification in drag of turbulent boundary layers resulting from manipulation of large-scale structures" NASA CR-3444.

Ganapathisubramani, B., Longmire, E. K., and Marusic, I. 2003. "Characteristics of vortex packets in turbulent boundary layers." *J. Fluid Mech.* **478**: 35–46.

Gao, Q., Ortiz-Dueñas, C., and Longmire E. K. 2011. "Analysis of vortex populations in turbulent wall-bounded flows." *J. Fluid Mech.* **678**:87–123.

Guala, M., Tomkins, C. D., Christensen, K. T., and Adrian, R.J. 2012. "Vortex organization in a turbulent boundary layer overlying sparse roughness elements." *Journal of Hydraulic Research* **50**:465–481.

Hain, R. Kähler, C.J. and Michaelis, C. 2008. "Tomographic and time resolved PIV measurements on a finite cylinder mounted on a flat plate." *Exp. Fluids* **45** (4):715–724.

Hutchins, N., Ganapathisubramani, B. & Marusic I. 2005. "Spanwise periodicity and the existence of very large scale coherence in turbulent boundary layers." *Turbulent Shear Flow Phenomena IV*, Williamsburg, VA.

Jacobi, I., and McKeon, B. J. 2011. "New perspectives on the impulsive roughness-perturbation of a turbulent boundary layer." *J. Fluid Mech.* **677**:179–203.

Nugroho, B., Hutchins, N., and Monty, J. P. 2013. "Large-scale spanwise periodicity in a turbulent boundary layer induced by highly ordered and directional surface roughness." *International Journal of Heat and Fluid Flow* **41**:90–102.

Ortiz-Dueñas, C., Ryan, M.D., and Longmire, E. K. 2011. "Modification of Turbulent Boundary Layer Structure Using Immersed Wall-Mounted Cylinders." *Proc. Turbulent Shear Flow Phenomena VIII*, Ottawa.

Park, C.W., Lee, S.J. 2000. "Free end effects on the near wake flow structure behind a finite cylinder mounted on a flat plate." *J. Wind Eng Ind Aerodyn.* **88**: 231 – 246.

Pattenden, R. J., Turnock, S.R. and Zhang, X. 2005. "Measurements of the flow over a low-aspect-ratio cylinder mounted on a ground plane." *Exp. Fluids* **39**(1):10–21.

Ryan, M.D., Ortiz-Dueñas, C., and Longmire, E. K. 2011. "Effects of Simple Wall-Mounted Cylinder Arrangements on a Turbulent Boundary Layer." *AIAA Journal.* **49**(10):2210–2220.

Sumner, D., Heseltine, J. L., and O. J. P. Dansereau. 2004. "Wake structure of a finite circular cylinder of small aspect ratio." *Exp. Fluids.* **37**:720–730.

Tan, Y. M., 2013. "Effect of an array of immersed array of cylinders in a turbulent boundary layer". Master's Report. University of Minnesota, Twin Cities.

Tomkins, C.D., 2001. "The structure of turbulence over smooth and rough walls". Ph.D. Thesis, University of Illinois at Urbana Champaign.

Tomkins, C.D., Adrian, R.J. 2003. "Spanwise structure and scale growth in turbulent boundary layers." *J. Fluid Mech.* **490**: 37-74.

Wang, H. F., Zhou, Y., Chan, C. K. and Lam, K.S. 2006. "Effect of initial conditions on interaction between a boundary layer and a wall-mounted finite-length-cylinder wake." *Phys. Fluids* **18**(6).

Zheng, S., and Longmire, E. K. 2014. "Perturbing vortex packets in a turbulent boundary layer." *J. Fluid Mech.* **748**:368–398.